

The stochastic background: scaling laws and time to detection for pulsar timing arrays

Xavier Siemens¹, Justin Ellis¹, Fredrick Jenet², Joseph D. Romano³

¹Center for Gravitation, Cosmology and Astrophysics, University of Wisconsin Milwaukee, PO Box 413, Milwaukee WI, 53201

²Department of Physics and Astronomy and Center for Advanced Radio Astronomy, University of Texas at Brownsville, Brownsville, TX 78520

³Department of Physics and Astronomy and Center for Gravitational-Wave Astronomy, University of Texas at Brownsville, Brownsville, TX 78520

E-mail: siemens@gravity.phys.uwm.edu

Abstract. We derive scaling laws for the signal-to-noise ratio of the optimal cross-correlation statistic, and show that the large power-law increase of the signal-to-noise ratio as a function of the observation time T that is usually assumed holds only at early times. After enough time has elapsed, pulsar timing arrays enter a new regime where the signal to noise only scales as \sqrt{T} . In addition, in this regime the quality of the pulsar timing data and the cadence become relatively un-important. This occurs because the lowest frequencies of the pulsar timing residuals become gravitational-wave dominated. Pulsar timing arrays enter this regime more quickly than one might naively suspect. For $T = 10$ yr observations and typical stochastic background amplitudes, pulsars with residual RMSs of less than about $1\ \mu\text{s}$ are already in that regime. The best strategy to increase the detectability of the background in this regime is to increase the number of pulsars in the array. We also perform realistic simulations of the NANOGrav pulsar timing array, which through an aggressive pulsar survey campaign adds new millisecond pulsars regularly to its array, and show that a detection is possible within a decade, and could occur as early as 2016.

1. Introduction

Pulsar timing arrays (PTAs) are sensitive to gravitational waves (GWs) in the nano-Hz band. The most promising sources at those frequencies are super-massive binary black holes (SMBBHs) that coalesce when galaxies merge. The superposition of GWs from the SMBBH mergers that have taken place throughout the history of the universe forms a stochastic background of gravitational waves [1–8]. These systems may also be observable through individual periodic signals [9–13] and bursts [14, 15]. A number of data analysis techniques have been implemented to search pulsar timing data for the stochastic background [16–30], periodic signals [31–38], and bursts [39].

Although the stochastic background produces random changes in the times-of-arrival (TOAs) of pulses from individual pulsars, its effects on the cross-correlation of timing residuals of two pulsars only depends on the angular separation between them [40]. In this paper we study the scaling properties of the optimal cross-correlation statistic introduced in [21]. This cross-correlation is optimized for the spectrum of the GW background, and accounts for the intrinsic noise of the pulsars. Using this

statistic we also calculate the detection probability for the NANOGrav pulsar timing array, finding that a detection could occur as early as 2016, and is likely before the end of the decade.

This paper is organized as follows. In Section 2 we review the cross-correlation statistic and its signal-to-noise ratio (SNR). In Section 3 we derive analytic scaling laws for the SNR of a simplified PTA as a function of the various properties and characteristics of the array. In Section 4 we perform realistic numerical simulations, including red spin noise, of the NANOGrav pulsar timing array. We conclude in Section 5.

2. The optimal cross-correlation statistic

In [30] we showed that for a timing array consisting of M pulsars, a simple linear (though non-invertible) transformation allows us to write the likelihood function for the residuals as a multivariate Gaussian

$$p(\mathbf{r}|\vec{\theta}) = \frac{1}{\sqrt{\det(2\pi\boldsymbol{\Sigma})}} \exp\left(-\frac{1}{2}\mathbf{r}^T\boldsymbol{\Sigma}^{-1}\mathbf{r}\right), \quad (1)$$

where

$$\mathbf{r} = \begin{bmatrix} r_1 \\ r_2 \\ \vdots \\ r_M \end{bmatrix} \quad (2)$$

is a vector of the timing residuals time-series, $r_I(t)$, for all pulsars, $\vec{\theta}$ is a vector of noise and signal parameters,

$$\boldsymbol{\Sigma} = \langle \mathbf{r}\mathbf{r}^T \rangle = \mathbf{R}\langle \mathbf{n}\mathbf{n}^T \rangle \mathbf{R}^T = \mathbf{R}\boldsymbol{\Sigma}_n\mathbf{R}^T \quad (3)$$

is the covariance matrix of the residuals, $\boldsymbol{\Sigma}_n$ is the covariance matrix for the pre-fit underlying Gaussian process \mathbf{n} which contains the gravitational waves along with other sources of noise, and

$$\mathbf{R} = \begin{bmatrix} R_1 & 0 & \dots & 0 \\ 0 & R_2 & \dots & 0 \\ \vdots & \vdots & \ddots & \vdots \\ 0 & 0 & \dots & R_M \end{bmatrix}. \quad (4)$$

is the timing model fitting matrix [41]. The covariance matrix for the timing residuals is the block matrix

$$\boldsymbol{\Sigma} = \begin{bmatrix} P_1 & S_{12} & \dots & S_{1M} \\ S_{21} & P_2 & \dots & S_{2M} \\ \vdots & \vdots & \ddots & \vdots \\ S_{M1} & S_{M2} & \dots & P_M \end{bmatrix}, \quad (5)$$

where

$$P_I = \langle r_I r_I^T \rangle, \quad (6)$$

$$S_{IJ} = \langle r_I r_J^T \rangle|_{I \neq J} \quad (7)$$

are the auto-covariance and cross-covariance matrices for each set of residuals. These matrices can be constructed by taking inverse Fourier transforms of the frequency domain auto- and cross-power spectra, and acting on them with the R -matrices,

$$\langle r_I r_I^T \rangle_{ij} = R_I \left[\int_{-\infty}^{\infty} df e^{2\pi i f(t_i - t_j)} P_I(f) \right] R_I^T \quad (8)$$

and

$$\langle r_I r_J^T \rangle_{ij} = \chi_{IJ} R_I \left[\int_{-\infty}^{\infty} df e^{2\pi i f(t_i - t_j)} P_g(f) \right] R_J^T \quad (9)$$

where ij are matrix component indices, $P_I(f)$ is the power spectrum of the I th pulsar, $P_g(f)$ is the GW power spectrum, and χ_{IJ} are the Hellings-Downs coefficients. This treatment is somewhat different from previous Bayesian analyses of the likelihood [14, 22, 24]. Our treatment amounts to a *conditional* pdf whereas [14, 22, 24] used a *marginalized* pdf. See [30] for more details.

In [21], we showed that in the weak-signal limit the likelihood ratio maximized over amplitudes leads to the optimal cross-correlation statistic for a PTA. The optimal statistic is

$$\hat{A}^2 = \frac{\sum_{IJ} r_I^T P_I^{-1} \tilde{S}_{IJ} P_J^{-1} r_J}{\sum_{IJ} \text{Tr} \left[P_I^{-1} \tilde{S}_{IJ} P_J^{-1} \tilde{S}_{JI} \right]}, \quad (10)$$

where \sum_{IJ} is the sum over all pulsar pairs. The normalization factor $\left(\sum_{IJ} \text{Tr} \left[P_I^{-1} \tilde{S}_{IJ} P_J^{-1} \tilde{S}_{JI} \right] \right)^{-1}$ is chosen so that \hat{A}^2 is also the maximum likelihood estimator for the amplitude of the stochastic background A^2 , and the amplitude independent cross-correlation matrix \tilde{S}_{IJ} is defined by

$$A^2 \tilde{S}_{IJ} = S_{IJ} = \langle r_I r_J^T \rangle. \quad (11)$$

In the absence of a cross-correlated signal (or if the signal is weak) the expectation value of \hat{A}^2 vanishes and its standard deviation is [21]

$$\sigma_0 = \left(\sum_{IJ} \text{Tr} \left[P_I^{-1} \tilde{S}_{IJ} P_J^{-1} \tilde{S}_{JI} \right] \right)^{-1/2}, \quad (12)$$

so if in a particular realization we measure a value \hat{A}^2 of the optimal statistic, the SNR for that realization is

$$\rho = \frac{\hat{A}^2}{\sigma_0} = \frac{\sum_{IJ} r_I^T P_I^{-1} \tilde{S}_{IJ} P_J^{-1} r_J}{\left(\sum_{IJ} \text{Tr} \left[P_I^{-1} \tilde{S}_{IJ} P_J^{-1} \tilde{S}_{JI} \right] \right)^{1/2}}. \quad (13)$$

This definition of the SNR measures our degree of surprise (in standard deviations away from 0), of finding cross-correlations in our data. The average SNR is

$$\langle \rho \rangle = A^2 \left(\sum_{IJ} \text{Tr} \left[P_I^{-1} \tilde{S}_{IJ} P_J^{-1} \tilde{S}_{JI} \right] \right)^{1/2}. \quad (14)$$

It is worth pointing out that this SNR only involves the cross-correlation terms of the likelihood, and does not include the auto-correlation terms. It is therefore

quite a stringent test of the presence of the stochastic background compared to, say, a likelihood based analysis that contains contributions to the likelihood from both auto- and cross-correlations [28–30, 42]. There is a very good reason for doing this: red noise in the auto-correlations could arise from intrinsic spin noise, frequency noise, or from propagation in the interstellar medium. The only way to be certain that we have detected a stochastic background of gravitational waves is to ensure the data are cross-correlated as we expect. From a Bayesian perspective we could achieve the same thing by comparing the evidence of a model with GW red noise (with correlated and uncorrelated components), with that of a model with only uncorrelated red noise. We can think of the SNR of the optimal cross-correlation statistic as a proxy for such an analysis.

3. Scaling laws for the cross-correlation statistic

Equation 14 for the SNR can be evaluated in the time domain for any PTA configuration (cadence, intrinsic red and white noises, etc.), along with a GW background amplitude and slope. The auto-covariance and cross-covariance matrices can be constructed by taking inverse Fourier transforms of the power spectra and cross-spectra, respectively, and accounting for fitting of the timing model in the time-domain as shown in Eqs. 8 and 9.

To understand how the SNR scales with the various properties of the PTA, however, it is easier to work in the frequency domain. The timing model, involves, among other things, subtracting out a quadratic (by fitting the period and period derivative out of the TOAs). In the frequency domain this can be crudely approximated by a low frequency cutoff at $f_L = 1/T$, where T is the time-span of the data. We can express the trace in the sum of Eq. 14 in the frequency domain as follows [21]

$$\text{Tr} \left[P_I^{-1} \tilde{S}_{IJ} P_J^{-1} \tilde{S}_{JI} \right] = \frac{2\chi_{IJ}^2 T}{A^4} \int_{f_L}^{f_H} df \frac{P_g^2(f)}{P_I(f)P_J(f)} \quad (15)$$

where χ_{IJ} are the Hellings Downs coefficients and the gravitational wave spectrum is

$$P_g(f) = \frac{A^2}{24\pi^2} \left(\frac{f}{f_{\text{ref}}} \right)^{2\alpha} f^{-3} = bf^{-\beta}, \quad (16)$$

where f_{ref} is some reference frequency which we will take here to be 1 yr. This means we can write the average SNR for the PTA as

$$\langle \rho \rangle = \left(2T \sum_{IJ} \chi_{IJ}^2 \int_{f_L}^{f_H} df \frac{P_g^2(f)}{P_I(f)P_J(f)} \right)^{1/2}. \quad (17)$$

If we assume there is only white noise in our pulsars (in addition to GWs), and that the data are evenly sampled with cadence $c = 1/\Delta t$, namely $P_I(f) = P_g(f) + 2\sigma_I^2 \Delta t$,

the integral in Eq. 17 can be written in terms of hypergeometric functions as follows

$$\begin{aligned} & \int_{f_L}^{f_H} df \frac{b^2 f^{-2\beta}}{(bf^{-\beta} + 2\sigma_I^2 \Delta t)(bf^{-\beta} + 2\sigma_J^2 \Delta t)} = \frac{1}{\sigma_I^2 - \sigma_J^2} \\ & \times \left[f_H \sigma_I^2 G\left(-\frac{2\Delta t f_H^\beta \sigma_I^2}{b}\right) - f_L \sigma_I^2 G\left(-\frac{2\Delta t f_L^\beta \sigma_I^2}{b}\right) \right. \\ & \left. - f_H \sigma_J^2 G\left(-\frac{2\Delta t f_H^\beta \sigma_J^2}{b}\right) + f_L \sigma_J^2 G\left(-\frac{2\Delta t f_L^\beta \sigma_J^2}{b}\right) \right], \end{aligned} \quad (18)$$

where $G(x) = {}_2F_1(1, \beta^{-1}, 1 + \beta^{-1}, x)$, and ${}_2F_1$ is the hypergeometric function. We will investigate the use of these solutions in future work.

For now let's consider the more simple situation where all the pulsars in our timing array have the same intrinsic white noise with RMS σ , and that the data are evenly sampled with cadence $c = 1/\Delta t$, i.e. we let $P_I(f) = P_J(f) = P(f) = P_g(f) + 2\sigma^2 \Delta t$. This means the average SNR can be written as the product

$$\langle \rho \rangle = \left(\sum_{IJ} \chi_{IJ}^2 \right)^{1/2} \left(2T \int_{f_L}^{f_H} df \frac{b^2 f^{-2\beta}}{(bf^{-\beta} + 2\sigma^2 \Delta t)^2} \right)^{1/2}. \quad (19)$$

It follows from this expression that the average SNR scales like the number of pulsars M in the timing array, since $\langle \rho \rangle \propto (\sum_{IJ} \chi_{IJ}^2)^{1/2} \propto M$. The integral we need to evaluate in Eq. 19 is

$$\int_{f_L}^{f_H} df \frac{b^2 f^{-2\beta}}{(bf^{-\beta} + 2\sigma^2 \Delta t)^2}, \quad (20)$$

which we show below can be expressed in terms of hypergeometric functions.

Before we do this, it is useful to consider two regimes in which Eq. 20 can be easily evaluated. The first is the *weak-signal limit* where the intrinsic white noise dominates $2\sigma^2 \Delta t \gg bf^{-\beta}$ for all frequencies $f \in [f_L, f_H]$. In this case Eq. 20 becomes,

$$\frac{b^2}{(2\sigma^2 \Delta t)^2} \int_{f_L}^{f_H} df f^{-2\beta} \approx \frac{b^2}{(2\sigma^2 \Delta t)^2} \frac{T^{2\beta-1}}{2\beta-1}, \quad (21)$$

because $f_L = 1/T$, so that the SNR becomes

$$\langle \rho \rangle = \left(\sum_{IJ} \chi_{IJ}^2 \right)^{1/2} \frac{bcT^\beta}{\sigma^2 \sqrt{(4\beta-2)}}. \quad (22)$$

The opposite regime, the *strong-signal limit*, occurs when the GW power is larger than the white noise, $2\sigma^2 \Delta t \ll bf^{-\beta}$, for all frequencies $f \in [f_L, f_H]$. In this case Eq. 20 simply becomes,

$$\int_{f_L}^{f_H} df \approx f_H = \frac{1}{2\Delta t} = \frac{c}{2}, \quad (23)$$

where we've set the high frequency cutoff f_H to be the Nyquist frequency. So the SNR becomes

$$\langle \rho \rangle = \left(\sum_{IJ} \chi_{IJ}^2 \right)^{1/2} (cT)^{1/2}. \quad (24)$$

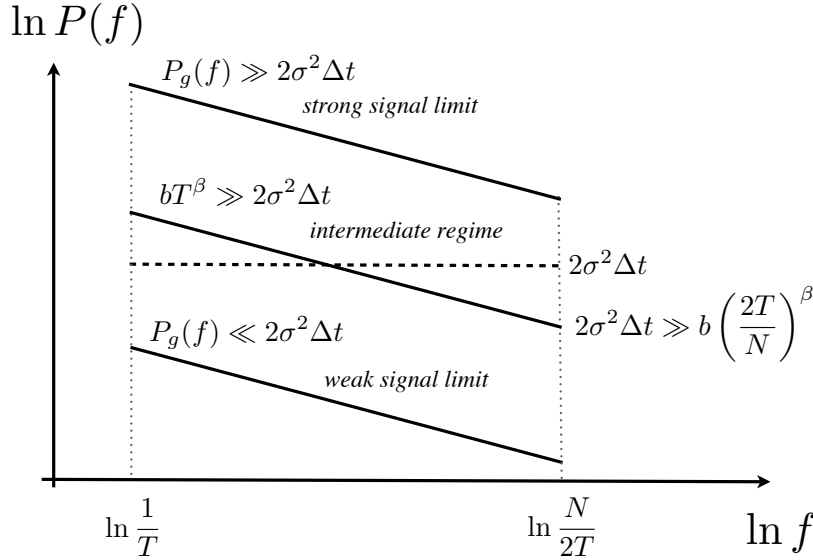


Figure 1. Schematic of the three scaling regimes. The weak-signal limit, where Eq. 22 is valid, is appropriate when the power spectrum of the stochastic background is lower than the white noise for all frequencies. The strong-signal limit, where Eq. 24 is valid, is appropriate in the opposite limit, when the power spectrum of the background is larger than the white noise at all frequencies. The intermediate regime, where Eq. 27 is valid, is appropriate when the lowest frequencies of the background are above the white noise level.

There is an *intermediate regime*, where the low frequencies of the background are above the white noise level, but the highest frequencies are below it. In this regime $P_g(f_L) = bT^\beta \gg 2\sigma^2\Delta t$ and $2\sigma^2\Delta t \gg b(2T/N)^\beta = P_g(f_H)$. The integral involved in the SNR calculation, Eq. 20, can be written as

$$\int_{f_L}^{f_H} df \frac{b^2 f^{-2\beta}}{(bf^{-\beta} + 2\sigma^2\Delta t)^2} = \int_0^{f_H} df \frac{b^2 f^{-2\beta}}{(bf^{-\beta} + 2\sigma^2\Delta t)^2} - \int_0^{f_L} df \frac{b^2 f^{-2\beta}}{(bf^{-\beta} + 2\sigma^2\Delta t)^2}, \quad (25)$$

and each of these integrals evaluated via

$$\int_0^{f_*} df \frac{b^2 f^{-2\beta}}{(bf^{-\beta} + 2\sigma^2\Delta t)^2} = \frac{f_*}{\beta} \left(\frac{1}{1 + \frac{2\sigma^2\Delta t f_*^\beta}{b}} + (\beta - 1) {}_2F_1(1, \beta^{-1}, 1 + \beta^{-1}, -\frac{2\sigma^2\Delta t f_*^\beta}{b}) \right). \quad (26)$$

The argument of the hypergeometric function for the second integral of the RHS of Eq. 25 is small, and the hypergeometric function can be approximated to be unity. For the first integral, the situation is somewhat more complicated, the argument is large and we need to make an asymptotic expansion of the hypergeometric function.

We give details of this calculation elsewhere [43], but the result is

$$\langle \rho \rangle = \left(\sum_{IJ} \chi_{IJ}^2 \right)^{1/2} \left[2 \left(\alpha \left(\frac{bc}{2\sigma^2} \right)^{1/\beta} T - 1 \right) \right]^{1/2}, \quad (27)$$

where

$$\alpha = \frac{\beta - 1}{\beta} \Gamma(1 - \beta^{-1}) \Gamma(1 + \beta^{-1}). \quad (28)$$

Figure 1 shows a plot of the gravitational wave power spectrum for all three regimes as well as the white noise. The transition from the weak signal regime to the intermediate regime occurs when the lowest frequency bin of the background becomes larger than the level of the white noise, i.e. when $bT^\beta > 2\Delta t\sigma^2$, the condition on the RMS is then

$$\sigma < \frac{A}{\pi} \sqrt{\frac{cT^\beta}{48}}. \quad (29)$$

For typical pulsar timing experiment durations of $T = 5$ yr, and cadence of about $c = 20$ yr⁻¹, for a background with amplitude $A = 10^{-15}$ and a spectral index like the one we expect for the SMBBH background ($\beta = 13/3$), the pulsar timing array is in the weak signal limit only if the pulsars have white noise RMSs greater than about 215 ns. Note that of the 17 pulsars analyzed in the 5 yr data set analyzed in [26], 9 have residuals with RMSs smaller than 215 ns.

Pulsar timing arrays currently have at least a few pulsars with RMS residuals considerably smaller than that, and Eq. 22 cannot be used. Table 1 shows the white noise RMS thresholds between the weak and intermediate regimes for low-, mid-, and upper ranges of the amplitude of the background and observation times T of 5, 10, 15, and 20 years.

It is worth pointing out that even though the lowest frequencies of the GW background may be larger than the white noise, the red noise induced residuals need not be large. The red noise induced residuals are

$$\sigma_{\text{red}}^2 = \int_{f_L}^{f_H} df b f^{-\beta} \approx \frac{bT^{\beta-1}}{\beta-1}, \quad (30)$$

for $\beta > 1$, so

$$\sigma_{\text{red}} \approx \frac{A}{\pi} \sqrt{\frac{T^{\beta-1}}{24(\beta-1)}}. \quad (31)$$

For $A = 10^{-15}$, $\beta = 13/3$, and $T = 5$ yr, the red noise induced RMS is $\sigma_{\text{red}} \approx 17$ ns, which is considerably smaller than the 215 ns RMS of *white* noise below which we enter the intermediate regime (see Table 1). Note that the pulsar with the smallest residuals analyzed in [26], J1713+0747, had a timing residual RMS of 30 ns.

In practice the strong-signal regime is irrelevant. We enter this regime when the highest frequency bin of the background is larger than the white noise, i.e. that $b(2T/N)^\beta > 2\Delta t\sigma^2$. In terms of the RMS this condition is

$$\sigma < \frac{A}{\pi} \sqrt{\frac{1}{24}} \left(\frac{2}{c} \right)^{(\beta-1)/2}. \quad (32)$$

Using a cadence of $c = 20$ yr⁻¹, for a background with amplitude $A = 10^{-15}$ and a spectral index like the one we expect for the SMBBH background, $\beta = 13/3$, the

	5 yr	10 yr	15 yr	20 yr
5.6×10^{-16}	120 ns	540 ns	1.3 μ s	2.4 μ s
1×10^{-15}	215 ns	965 ns	2.3 μ s	4.3 μ s
2×10^{-15}	430 ns	1.9 μ s	4.6 μ s	8.7 μ s

Table 1. White noise RMS values (using Eq. 29) at which we transition from the weak-signal limit to the intermediate regime for low, mid-range, and upper values of the SMBBH background [7], $\beta = 13/3$, and four observation times. We have taken the cadence to be $c = 20 \text{ yr}^{-1}$. PTA data time-spans are now reaching 20 yrs, so pulsars with white noise levels of less than a few μ s are already in the intermediate regime.

condition on the RMS is $\sigma < 4.3 \times 10^{-11}$ s. The constraint can be loosened only by reducing the cadence, which reduces the highest frequencies probed by the experiment.

To summarize, the SNR scales with PTA characteristics in two different ways depending on whether the lowest frequencies of the stochastic background power spectrum are above or below the white noise level. When $P_g(f) \ll 2\sigma^2\Delta t$ for all frequencies $f \in [f_L, f_H]$ the SNR is given by

$$\langle \rho \rangle = \left(\sum_{IJ} \chi_{IJ}^2 \right)^{1/2} \frac{bcT^\beta}{\sigma^2 \sqrt{(4\beta - 2)}} \propto Mc \frac{A^2}{\sigma^2} T^\beta. \quad (33)$$

If the PTA begins in this regime, after enough time passes, the condition $bT^\beta < 2\Delta t\sigma^2$ is no longer satisfied and the lowest frequency bins of the background become larger than the white noise. At this stage the SNR scaling changes to

$$\langle \rho \rangle = \left(\sum_{IJ} \chi_{IJ}^2 \right)^{1/2} \left[2 \left(\alpha \left(\frac{bc}{2\sigma^2} \right)^{1/\beta} T - 1 \right) \right]^{1/2} \propto M \left(\frac{A}{\sigma\sqrt{c}} \right)^{1/\beta} T^{1/2}, \quad (34)$$

with α given by Eq. 28. Table 1 shows the white noise RMS thresholds below which Eq. 34 should be used for various observation times and amplitudes of the background.

Figure 2 shows the average SNR versus time for a GW stochastic background calculated in the time domain with Eq. 14, with $A = 10^{-15}$, $M = 20$, $c = 20 \text{ yr}^{-1}$, $\sigma = 100$ ns along with the two scaling laws Eqs. 33 and 34 at late times. For the timing model we have used quadratic subtraction (fitting for an overall phase, period, and period derivative). In our frequency domain derivation we approximated the fitting of the timing model with a low frequency cutoff of $f_L = 1/T$. In this plot we have taken $T \rightarrow 1.55T$ for both Eq. 33 and 34 which reflects the fact that working in the frequency domain with a low frequency cutoff at $1/T$ does not capture the effects of the timing model completely, though it gives the correct dependence on the PTA parameters.

The difference in the dependence on the observation time, cadence, white noise RMS of the pulsars, and amplitude of the background of the two regimes is striking, and critical for PTA optimization. The combination bc/σ^2 appears in both cases but with two different powers. While increasing the cadence and improving the white noise RMS helps greatly in the weak signal limit, their impact on the SNR in the intermediate regime is not as significant. The reason for this is that the SNR is dominated by the lowest frequency bins. When these bins become gravitational-wave dominated, the dominant contribution to the noise is the uncorrelated pulsar-term

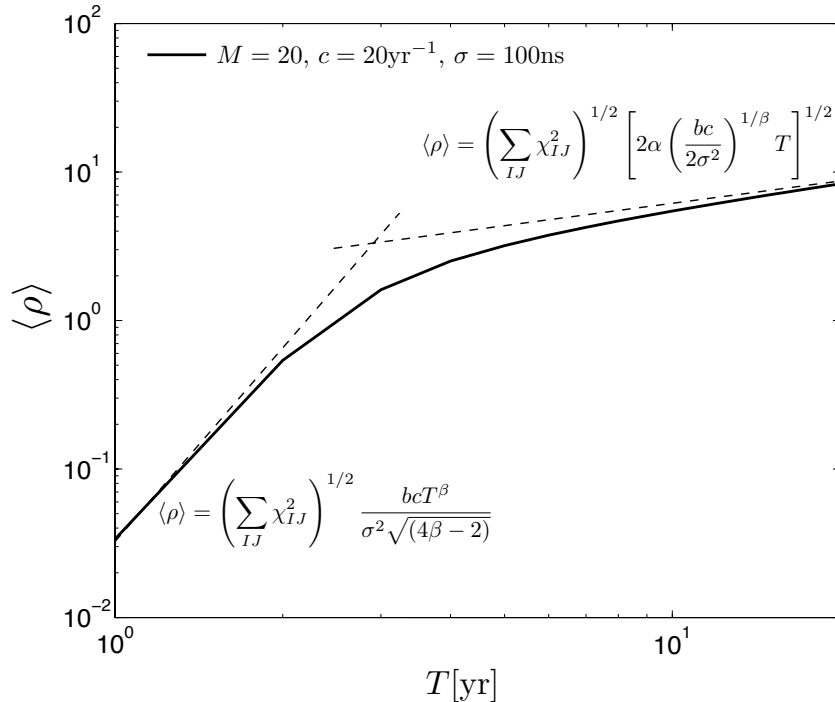


Figure 2. Plot of the SNR versus time in years for a stochastic background with amplitude $A = 10^{-15}$, $M = 20$, $c = 20 \text{ yr}^{-1}$, $\sigma = 100 \text{ ns}$. The solid curve is computed using Eq. 14 in the time domain using a quadratic subtraction timing model. The dashed curves are computed using Eqs. 33 and 34 at late times as indicated in the plot. Approximating the timing model with a low frequency cutoff of $f_L = 1/T$ is not quite correct, though it does yield the correct dependence on the various PTA properties. In this plot we took $T \rightarrow 1.55T$ for both Eq. 33 and 34.

GW red noise, rather than the white noise, and this changes the scaling dramatically: the un-correlated part of the gravitational-wave stochastic background is interfering with our ability to detect the correlated piece via cross-correlations. The most effective way to beat down the uncorrelated part of the GW signal is to add more pulsars to the PTA.

PTA data sets are now reaching 20 year time spans with pulsar RMSs at the level of a few μs , so the regime where Eq. 34 is valid is probably already relevant or will soon be. This is critical when considering the kinds of decisions the pulsar timing community will have to make in terms of observing strategies to ensure a prompt and confident detection of the stochastic GW background.

In Fig. 3 we illustrate this point. We plot the SNR for a number of different PTA configurations and a SMBBH stochastic background with amplitude $A = 10^{-15}$ and slope $\beta = 13/3$. The canonical PTA configuration, with $M = 20$ pulsars with $\sigma = 100 \text{ ns}$, and a cadence of $c = 20 \text{ yr}^{-1}$ is shown in gray. The dashed curve shows the same PTA with a cadence of $c = 5 \text{ yr}^{-1}$, and though at early times the SNR for the gray higher-cadence curve is larger than the dashed curve, at late times the cadence becomes un-important as can be gleaned from Eqs. 33 and 34. The solid curve shows

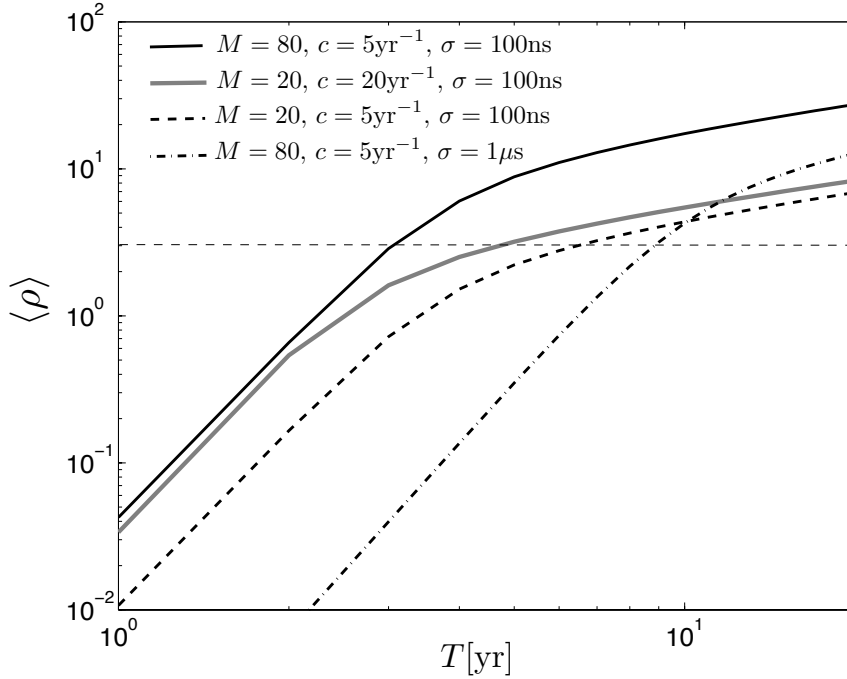


Figure 3. SNR versus time in years for various PTA configurations and an amplitude of the stochastic background of $A = 10^{-15}$. The solid curve shows a PTA with 80 pulsars, timed at a cadence of 5 points per year and an RMS of 100 ns. The gray curve shows a PTA with 20 pulsars, an RMS of 100 ns, and a cadence of 20 points per year. The dashed curve shows the same PTA with cadence of 5 points per year. Though at early times the SNR for the gray curve is larger than the dashed curve, at late times the cadence becomes un-important and the two SNRs become comparable, as can be seen from Eqs. 33 and 34. The dash-dot curve shows a PTA with 80 pulsars with $1 \mu\text{s}$ residuals and a cadence of 5 point per year. Though initially this PTA has a smaller SNR than the 20 pulsar PTAs, at late times it leads to a larger SNR.

a PTA with $M = 80$ pulsars timed with a cadence of 5 points per year and an RMS of $\sigma = 100$ ns. Both solid curves involve the same total observation time ($cM = 400$). More pulsars and smaller cadence lead to an SNR that is significantly greater and a more confident detection in the long term. The dash-dot curve shows a PTA with $M = 80$ pulsars with $\sigma = 1 \mu\text{s}$ residuals and a cadence c of 5 point per year. Though initially this PTA has a smaller SNR than the 20 pulsar PTAs, at late times it leads to a larger SNR because the RMS and cadence become unimportant compared to the number of pulsars.

The work we have described in this section began with our attempts to understand (through simulations) the time it would take a realistic PTA to detect the gravitational-wave background. We expected that the weak-signal approximation would be valid for all times, and in particular that we would benefit from the dramatic increase in the SNR with time as predicted by Eq. 33. What we found instead was that after some time the SNR grows only as the square root of the observing time. The

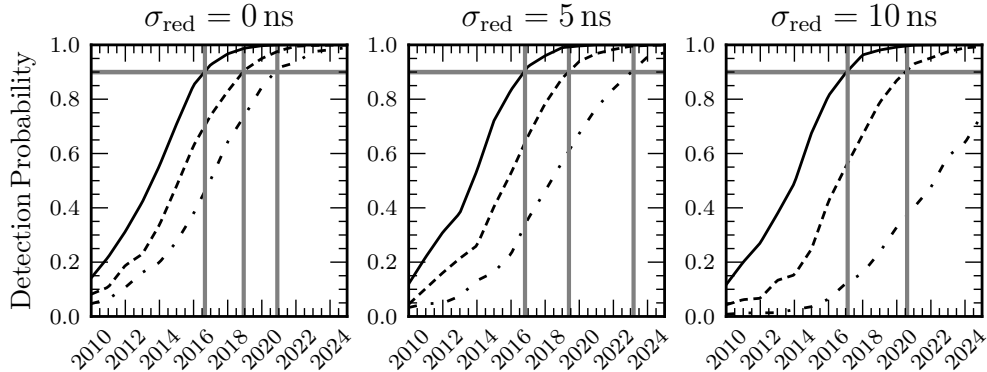


Figure 4. Detection probability versus time in years for the NANOGrav pulsar timing array. We show the detection probability for 3 different amplitudes $A = 5.6 \times 10^{-16}$ (dash-dot), $A = 1 \times 10^{-15}$ (dashed), and $A = 2 \times 10^{-15}$ (solid) of the stochastic background generated by supermassive binary black holes [7]. We have used the combined epoch RMSs of the 17 pulsars in [26], started timing 35 total pulsars in 2013, and added 3 new pulsars per year with an epoch combined RMS of 200 ns prior to hardware improvements (this is the median of the 17 pulsars in [26]).

reason for that, we now understand, is that the PTA enters the intermediate regime.

4. Time to detection for realistic pulsar timing arrays

In this section we discuss the detection potential of the NANOGrav pulsar timing array [44]. NANOGrav started collecting data on 17 millisecond pulsars in 2005, and upper limits on the GW background using these pulsars timed up to 2010 were published last year [26]. Through various surveys, NANOGrav has since increased the number of pulsars timed to 35, at about a rate of 3 new pulsars added every year. About half of the pulsars are timed at Green Bank, and the other half at Arecibo.

In our simulations we have used the epoch-averaged combined residuals for the 17 pulsars in Table 2 of [26]. New high-bandwidth pulsar timing back-ends have been installed at the Green Bank Telescope (in 2010), and Arecibo (in 2012). The new back ends have a bandwidth that is about a factor of 10 larger than the previous ones, and we might expect an increase in TOA precision of about a factor of 3. In fact, on average only about a factor of 2 improvement has been observed, presumably due to jitter noise [45]. In our simulations we have assumed a factor of 2 improvement from the new hardware starting in 2010 for pulsars timed at Green Bank and 2012 for pulsars timed at Arecibo. For new pulsars added to the array we have assumed an epoch combined RMS of 200 ns prior to hardware improvements (this is the median of the 17 pulsars in [26]). We have taken conservative lower ($A = 5.6 \times 10^{-16}$), middle ($A = 1 \times 10^{-15}$), and upper ($A = 2 \times 10^{-15}$) values for the amplitude of the stochastic background generated by supermassive binary black holes [7]. At each time we perform 1000 injections of simulated signals. The detection probability is the fraction of injections that exceed an SNR of 3. The variance of the SNR is quite large in the presence of a signal [43], so looking at the SNR threshold alone is not

sufficient, and the 90% detection probability is typically reached when the average SNR is significantly larger than 3.

Although most NANOGrav pulsars do not show strong evidence of red noise, in our simulations we have included the effects of red spin noise (with spectral index of -5) [45]. We resort to simulations for this because we have not found a means to include the effects of this type of noise into our analytic estimates of the SNR.

Figure 4 shows the results of our simulations. The three panels show red spin noise that induces an RMS of 0 ns, 5 ns, and 10 ns at 5 yrs. The figure shows that for all but the most pessimistic scenario (lowest amplitude and largest intrinsic spin noise), a detection will occur by 2023, and could occur as early as 2016.

This prompt detection is possible because of the addition of new pulsars to the timing array. The importance of adding new pulsars is illustrated in Fig. 5. The top three panels show the detection probability as a function of time for the 17 pulsars in [26], but adding no additional pulsars. The bottom three panels show a pulsar timing array with just 6 pulsars, with white noise RMSs of 10 ns. Clearly, increasing the number of pulsars is critical to our ability to confidently detect the stochastic background.

5. Summary

We have produced analytic expressions for the SNR of the optimal cross-correlation statistic for stochastic background searches as a function of the various PTA properties. We find that the weak signal limit scalings where $\langle \rho \rangle \propto T^\beta$ do not apply at all times. Once enough time has elapsed the lowest frequencies of pulsar timing residuals become GW-dominated and the scaling changes to $\langle \rho \rangle \propto \sqrt{T}$. In addition, the dependence on the cadence and the RMS of the residuals weakens significantly, and the best strategy to confidently detect the stochastic background is to increase the number of pulsars in the PTA.

PTAs may enter this new regime more quickly than one might have thought naively. Of the 17 pulsars in the 5 year data set analyzed in [26], 9 are already in this regime for typical values of the amplitude of the stochastic background ($A \sim 10^{-15}$). Some current PTA data sets span close to 20 yrs, and for the same amplitude of the background their lowest frequency bins are GW-dominated if the RMSs of the timing residuals are smaller than a few μs .

We have also made realistic simulations of the NANOGrav PTA. NANOGrav is currently timing 35 pulsars and adding more to its array at a rate of about 3 per year. Where possible, we have used the measured RMSs of millisecond pulsars, and for future discoveries we have used the median RMS of the existing set. Most NANOGrav pulsars do not show strong evidence for intrinsic red noise. Nevertheless, to be conservative, we have included the effects of red spin noise in our simulations. We find that a confident detection of the background could occur as early as 2016.

It is worth pointing out that although for stochastic background searches the RMS of timing residuals becomes un-important at late times, there are very good reasons to improve on the RMS of pulsars. For example, for other types of GW signals such as continuous waves and bursts, the sensitivity is dominated by the pulsars with the smallest residuals.

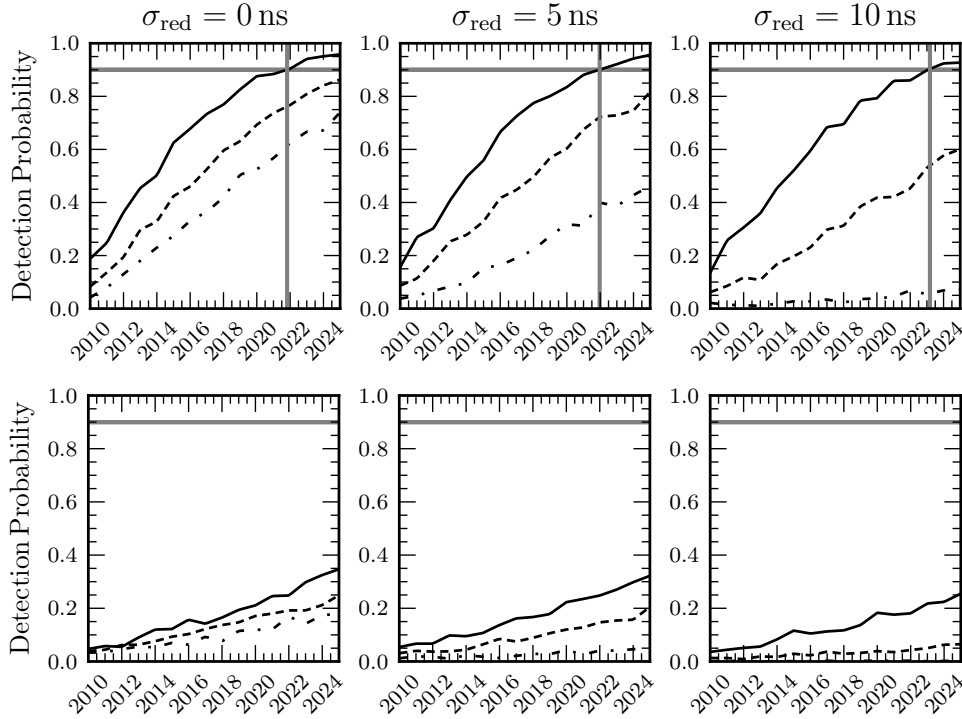


Figure 5. Detection probability as a function of time for the 17 NANOGrav pulsars of [26], but adding no additional pulsars to the array (top three panels). Detection probability as a function of time for a pulsar timing array with just 6 pulsars with white noise RMSs of 10 ns (bottom three panels). The detection probability is shown for 3 different amplitudes $A = 5.6 \times 10^{-16}$ (dash-dot), $A = 1 \times 10^{-15}$ (dashed), and $A = 2 \times 10^{-15}$ (solid) of the stochastic background generated by supermassive binary black holes [7].

Acknowledgments

We would like to thank Jim Cordes, Paul Demorest, Scott Ransom, Rutger van Haasteren, and the members of the NANOGrav detection working group for their comments and support. The work of XS and JE was partially funded by the NSF through CAREER award number 0955929, PIRE award number 0968126, award number 0970074, and the Wisconsin Space Grant Consortium. JDR would like to acknowledge NSF award CREST-0734800.

References

- [1] Lommen A N and Backer D C 2001 *ApJ* **562** 297–302
- [2] Jaffe A H and Backer D C 2003 *ApJ* **583** 616–631
- [3] Wytthe J S B and Loeb A 2003 *ApJ* **590** 691–706
- [4] Volonteri M, Haardt F and Madau P 2003 *ApJ* **582** 559–573

- [5] Enoki M, Inoue K T, Nagashima M and Sugiyama N 2004 *ApJ* **615** 19–28
- [6] Sesana A, Vecchio A and Colacino C N 2008 *MNRAS* **390** 192–209
- [7] Sesana A 2012 *arXiv:1211.5375*
- [8] McWilliams S T, Ostriker J P and Pretorius F 2012
- [9] Sesana A, Vecchio A and Volonteri M 2009 *MNRAS* **394** 2255–2265
- [10] Sesana A and Vecchio A 2010 *Phys. Rev. D* **81** 104008–+
- [11] Roedig C and Sesana A 2011 *arXiv:1111.3742*
- [12] Ravi V, Wyithe J S B, Hobbs G, Shannon R M, Manchester R N, Yardley D R B and Keith M J 2012
- [13] Mingarelli C, Grover K, Sidery T, Smith R and Vecchio A 2012 *Phys.Rev.Lett.* **109** 081104
- [14] van Haasteren R and Levin Y 2010 *MNRAS* **401** 2372–2378
- [15] Cordes J and Jenet F 2012 *Astrophys.J.* **752** 54
- [16] Detweiler S 1979 *ApJ* **234** 1100–1104
- [17] Stinebring D R, Ryba M F, Taylor J H and Romani R W 1990 *Physical Review Letters* **65** 285–288
- [18] Lommen A N 2002 *Neutron Stars, Pulsars, and Supernova Remnants* ed W Becker, H Lesch, & J Trümper pp 114–+ (*Preprint arXiv:astro-ph/0208572*)
- [19] Jenet F A, Hobbs G B, Lee K J and Manchester R N 2005 *ApJL* **625** L123–L126
- [20] Jenet F A, Hobbs G B, van Straten W, Manchester R N, Bailes M, Verbiest J P W, Edwards R T, Hotan A W, Sarkissian J M and Ord S M 2006 *ApJ* **653** 1571–1576
- [21] Anholm M, Ballmer S, Creighton J D E, Price L R and Siemens X 2009 *Phys. Rev. D* **79** 084030–+
- [22] van Haasteren R, Levin Y, McDonald P and Lu T 2009 *MNRAS* **395** 1005–1014
- [23] Yardley D R B, Coles W A, Hobbs G B, Verbiest J P W, Manchester R N, van Straten W, Jenet F A, Bailes M, Bhat N D R, Burke-Spolaor S, Champion D J, Hotan A W, Oslowski S, Reynolds J E and Sarkissian J M 2011 *MNRAS* **414** 1777–1787
- [24] van Haasteren R, Levin Y, Janssen G H, Lazaridis K, Kramer M, Stappers B W, Desvignes G, Purver M B, Lyne A G, Ferdman R D, Jessner A, Cognard I, Theureau G, D’Amico N, Possenti A, Burgay M, Corongiu A, Hessels J W T, Smits R and Verbiest J P W 2011 *MNRAS* **414** 3117–3128
- [25] Cordes J and Shannon R 2012 *Astrophys.J.* **750** 89
- [26] Demorest P B, Ferdman R D, Gonzalez M E, Nice D, Ransom S, Stairs I H, Arzoumanian Z, Brazier A, Burke-Spolaor S, Chamberlin S J, Cordes J M, Ellis J, Finn L S, Freire P, Giampanis S, Jenet F, Kaspi V M, Lazio J, Lommen A N, McLaughlin M, Palliyaguru N, Perrodin D, Shannon R M, Siemens X, Stinebring D, Swiggum J and Zhu W W 2012 *Astrophys.J.* **762** (2013) 94
- [27] van Haasteren R 2013 *MNRAS* **429** 55–62
- [28] Lentati L, Alexander P, Hobson M P, Taylor S and Balan S T 2012
- [29] Taylor S R, Gair J R and Lentati L 2012
- [30] Ellis J, Siemens X and van Haasteren R 2013 *ArXiv e-prints*
- [31] Jenet F A, Lommen A, Larson S L and Wen L 2004 *ApJ* **606** 799–803
- [32] Yardley D R B, Hobbs G B, Jenet F A, Verbiest J P W, Wen Z L, Manchester R N, Coles W A, van Straten W, Bailes M, Bhat N D R, Burke-Spolaor S, Champion D J, Hotan A W and Sarkissian J M 2010 *MNRAS* **407** 669–680
- [33] Corbin V and Cornish N J 2010 *arXiv:1008.1782*
- [34] Lee K J, Wex N, Kramer M, Stappers B W, Bassa C G, Janssen G H, Karuppusamy R and Smits R 2011 *MNRAS* **414** 3251–3264
- [35] Ellis J A, Jenet F A and McLaughlin M A 2012 *ApJ* **753** 96
- [36] Babak S and Sesana A 2012 *Phys. Rev. D* **85** 044034
- [37] Ellis J A, Siemens X and Creighton J D E 2012 *ApJ* **756** 175
- [38] Petiteau A, Babak S, Sesana A and de Araújo M 2013 *Phys. Rev. D* **87**(6) 064036 URL <http://link.aps.org/doi/10.1103/PhysRevD.87.064036>
- [39] Finn L S and Lommen A N 2010 *ApJ* **718** 1400–1415
- [40] Hellings R W and Downs G S 1983 *ApJL* **265** L39–L42
- [41] Demorest P B 2007 *Measuring the gravitational wave background using precision pulsar timing* Ph.D. thesis University of California, Berkeley
- [42] van Haasteren R, Levin Y, McDonald P and Lu T 2009 *MNRAS* **395** 1005–1014
- [43] S Chamberlin J Creighton P D J E J R X S 2013 *In preparation*
- [44] Jenet F, Finn L S, Lazio J, Lommen A, McLaughlin M, Stairs I, Stinebring D, Verbiest J, Archibald A, Arzoumanian Z, Backer D, Cordes J, Demorest P, Ferdman R, Freire P, Gonzalez M, Kaspi V, Kondratiev V, Lorimer D, Lynch R, Nice D, Ransom S, Shannon R and Siemens

*The stochastic background: scaling laws and time to detection for pulsar timing arrays*15

X 2009 *arXiv:0909.1058*

[45] Cordes J M and Shannon R M 2012 *ApJ* **750** 89